



MODELING ELECTROHYDRODYNAMICALLY ENHANCED DRAG IN CHANNEL AND PIPE FLOWS USING ONE-DIMENSIONAL TURBULENCE

Marten KLEIN¹, Juan Alí MEDINA MÉNDEZ¹, Heiko SCHMIDT¹

¹ Chair of Numerical Fluid and Gas Dynamics, Faculty of Mechanical Engineering, Electrical and Energy Systems, Brandenburg University of Technology (BTU) Cottbus-Senftenberg. Siemens-Halske-Ring 15A, D-03046, Cottbus, Germany. Tel.: +49 355 69-5127, Fax: +49 355 69-5127, E-mail: marten.klein@b-tu.de (M. Klein), medinjua@b-tu.de (J. A. Medina Méndez), heiko.schmidt@b-tu.de (H. Schmidt)

ABSTRACT

The joint modeling of flow hydrodynamics and electrokinetics is a relatively unexplored area of turbulent flow research. We address a lack of available models for electrohydrodynamic (EHD) turbulent flow utilizing a lower-order approach, the stochastic One-Dimensional Turbulence (ODT) model. ODT is constructed on the principles of the direct energy cascade of Navier–Stokes turbulence, with key emphasis on the accurate resolution of the small molecular transport scales within a notional line-of-sight. We investigate two canonical flow configurations to demonstrate the applicability of the model in the simulation of EHD flows. First, we investigate EHD effects in zero-pressure-gradient turbulent boundary layers by two-way coupled model application to plane Couette flow of a dilute electrolyte. Second, we apply the one-way coupled model to EHD-enhanced gas flow through a vertical pipe with an inner concentric electrode, where electric fields are generated by means of a corona discharge and the corresponding effect of a continuum ionic charge density field.

Keywords: EHD turbulence, multiphysical boundary layers, one-dimensional turbulence, stochastic modeling, turbulent drag

1. INTRODUCTION

Electrohydrodynamic (EHD) flows are encountered in various technical applications. As an overview of research-led EHD applications we cite examples of electrostatic precipitation [1], EHD-enhancement of heat and mass transfer [2, 3], turbulent drag [4], hydrogen production in water electrolysis [5], plasma-assisted combustion [6], among others. For numerical simulations of such devices, it is crucial to accurately and economically model entangled hydrodynamic and electrokinetic processes. One of the key issues to resolve for accurate modeling of EHD flows is the correct representation of nonlocal and nonlinear interactions between the fluid

flow, charge-carrier distributions, and electric fields. These interactions may cause a departure of the turbulence dynamics, e.g., from K41 [7] to electrokinetic turbulence [8]. Indeed, on some EHD regimes, turbulence may appear even at very low Reynolds numbers, e.g., when the electric body forces substitute the role of external inertial forces, and the former are in a large ratio with respect to the viscous forces [9]. Direct Numerical Simulations (DNSs) should be the method of preferred choice for unraveling the physics presents in EHD flows. However, DNSs are, even to this day, limited in terms of their heavy computational overload, i.e., limited to moderate Reynolds numbers [10]. Needless to say, diffusive sub-filter-scale parameterizations used in Reynolds-averaged Navier–Stokes (RANS) or large-eddy simulations (LES), specifically in the presence of walls, are of limited applicability in EHD flows. Alternative to filter-based turbulence models, we address issues in turbulent EHD flows with a dimensionally reduced stochastic modeling approach, One-Dimensional Turbulence (ODT) [11], due to its ability to faithfully represent fluctuating simultaneous scalar and momentum transport in the vicinity of a wall [12]. ODT aims to resolve all relevant scales of the flow but only for a notional line-of-sight. A stochastic process is used to mimic the effects of turbulent stirring motions, whereas deterministic molecular diffusion, electric drift currents, Coulomb forces, and boundary conditions, are directly resolved.

The rest of this paper is organized as follows. Section 2 gives an overview of the ODT model formulations for multiphysical wall-bounded flows with an extension to EHD flows. Section 3 collects key results partitioned into two-way coupled EHD Couette flow of dilute electrolytes and one-way coupled EHD-enhanced vertical pipe flow with an inner concentric electrode. Last, in Section 4, we summarize the two case studies.

2. FLOW MODEL FORMULATION

2.1. Overview of the ODT model

In decaying isotropic turbulence seen on a line-of-sight through the turbulent flow (the ODT line), piecewise-transformations on scalar profiles, or triplet maps, induce an increase in the rate of strain, which is characteristic of turbulent eddies. Symbolically, the effect of the triplet map $f(y)$ on an instantaneous profile of the property field $\psi(y)$ is denoted as the transformation $\psi(y) \rightarrow \psi(f(y))$ (in a y -oriented wall-normal domain of a Cartesian coordinate system) [11]. The triplet map microscopically models turbulence phenomenology. It takes a property profile along a selected size l interval, compresses the profile to $l/3$, pastes two copies of this profile to fill again, and flips the central copy to ensure continuity.

Such mapping events are stochastically sampled from unknown distribution functions with the aid of a Poisson process (e.g. [13]). Based on assumed distribution functions for the mapping event size l and location y_0 , an efficient thinning-and-rejection method is used for probabilistic selection, in which the rate of implementation of the mappings is calculated in accordance with the local turbulence time-scale (eddy turnover time τ). The latter is obtained from the available energy of the current flow state. Under absence of body forces, the available energy follows from the velocity shear across a size- l interval around location y_0 [11] since the eddy kinetic energy, l^2/τ^2 , is proportional to the squared eddy velocity, u_K^2 . This scale velocity is modified when eddy-available potential energy and viscous effects are taken into account as detailed below. A factor of proportionality that controls the rate of implemented mapping events is included in the model as a rate parameter, C . The kinetic energy and the rate-of-strain are related by means of an equivalent turbulent diffusivity. The implementation of a given map at fixed turbulent diffusivity then favors the sampling of further mappings. This is the model representation of the turbulent kinetic energy cascade [11].

The set of operations comprising the sampling process and the mappings themselves is known as an eddy event. For decaying isotropic turbulence, there are still two other elements required in the model to complete a consistent dynamic picture of turbulence. One is a mechanism for viscous transport implementation, and the other one is a mechanism for turbulence kinetic energy (TKE) dissipation. Both are a consequence of the viscous momentum flux, which is implemented in a direct way in ODT, by resolving the corresponding numerical fluxes in the 1-D domain after an eddy event has been sampled [11]. This leads to the formulation of a symbolic 1-D partial differential equation (PDE) for a scalar velocity component ψ in ODT. Specialized to Cartesian coordinates, this is

$$\frac{\partial \psi}{\partial t} = M - \frac{\partial F(\psi)}{\partial y}. \quad (1)$$

Here, $F(\psi)$ is the model-resolved flux of ψ , e.g., $F(\psi) = -\sigma(\partial\psi/\partial y)$ for molecular diffusive gradient fluxes in which σ is a kinematic diffusion coefficient. $M = M(C, y, f(y))$ represents discrete mapping effects that punctuate deterministic evolution of the conserved scalar $\psi(y, t)$ at discrete times. The mapping effects depend on the selected physical mapping $f(y)$, which models turbulent microstructure, and a turbulent eddy rate parameter C .

2.2. Model formulation for temporally developing planar wall-bounded flow

The presence of walls introduces a wall-normal-position dependence on the turbulent scalar transport. Close to the wall, viscous transport is dominantly one-dimensional, aligned with the wall-normal direction. Away from the wall, viscous transport may have a more inherent 3-D character, although the turbulent transport may dominate instead. The transition between the near-wall and away-from-the-wall behavior is controlled in ODT in practical terms by the model parameter Z . The latter defines a viscous penalty by setting a lower limit below which eddy implementation is suppressed [14]. This imposes the dominance of the viscous transport.

Another important dynamical feature in wall-bounded flows is the anisotropy of the velocity statistics. In this context, the role of the turbulent pressure transport is the redistribution of the TKE among the Reynolds stress components [15]. In ODT, this pressure-scrambling effect is modeled with the aid of a kernel function $K(y) = y - f(y)$ [14]. Eddy events are modified to implement mappings, as well as the kernel effects for velocity components, such that $\psi(y) \rightarrow \psi(f(y))$ for a conserved scalar, and $u_i(y) \rightarrow u_i(f(y)) + c_i(\alpha)K(y)$ for the Cartesian velocity components u_i , $i = 1, 2, 3$. As detailed in [14], c_i is a kernel coefficient calculated based on the available energy and a model parameter $\alpha \in [0, 1]$ that controls the efficiency of inter-component kinetic energy redistribution, such that

$$c_i = \frac{1}{\int_{y_0}^{y_0+l} \rho K^2 dy} \left[u_{i,K} + \text{sgn}(u_{i,K}) \times \sqrt{(1-\alpha)u_{i,K}^2 + \frac{\alpha}{2}(u_{j,K}^2 + u_{k,K}^2)} \right]. \quad (2)$$

Here, $u_{i,K} = \int_{y_0}^{y_0+l} \rho u_i(f(y))K(y) dy$, where ρ is the uniform density, and (i, j, k) permutations of $(1, 2, 3)$.

The expression for τ , or in this case τ^{-2} , considering $u_{i,K}$ as the available kinetic energy for redistribution, as well as the viscous penalty factor, is based on [14],

$$\tau^{-2} = \frac{2K_0}{\int_{y_0}^{y_0+l} \rho K^2(y) dy} \times \left[\frac{K_0 \sum_i u_{i,K}^2}{2 \int_{y_0}^{y_0+l} \rho K^2(y) dy} - \frac{Z}{2} \frac{\mu_{\text{eddy}}^2}{\rho_{\text{eddy}} l^2} \int_{y_0}^{y_0+l} dy \right]. \quad (3)$$

Here, $K_0 = \left(l^2 \int_{y_0}^{y_0+l} dy \right)^{-1} \int_{y_0}^{y_0+l} K^2(y) dy$, which converges to $4/27$ in the continuum kernel limit. Additionally, μ_{eddy} and ρ_{eddy} are weighted averages of the dynamic viscosity and the density within the eddy range $[y_0, y_0 + l]$. The density and dynamic viscosity of the fluid are assumed as constants, and of uniform value.

Eddy events are sampled in time on the basis of an acceptance probability p_a , following a Poisson process. p_a is calculated as in [11], considering the rate parameter, as

$$p_a = C \frac{\Delta t_s}{\tau} \frac{1}{l^2 \chi(l, y_0)} < 1. \quad (4)$$

Here, Δt_s is a sampling time interval which needs to be able to resolve any possible τ , such that, in general, $\Delta t_s < \tau$ (adapted dynamically, see [14]). $\chi(l, y_0)$ is a presumed joint probability density function (JPDF) of eddy event sizes and locations to obtain candidate events. Oversampling and rejection guarantees that ODT simulation results are insensitive to the exact choice of this JPDF.

After an eddy event is implemented, the deterministic evolution is comparable to that in Eq. (1). With the model resolved viscous flux $F_i(u_i) = -\nu(\partial u_i / \partial y)$, mapping (M_i) and kernel, as well as momentum sources for the selected component i , we obtain

$$\frac{\partial u_i}{\partial t} = M_i + K_i + S_i + \nu \frac{\partial^2 u_i}{\partial y^2}. \quad (5)$$

This expression incorporates now symbolically the effects of the kernel, and of the energy redistribution among velocity components, by means of the term $K_i(C, Z, \alpha, u, f(y))$. S_i is a source term for the i -th velocity component to be integrated together with the viscous flux, e.g., a fixed pressure gradient (FPG).

2.3. Extension to spatially developing flow with variable density effects

The model formulation presented in Section 2.2 considers the temporal change of scalar profiles along a line-of-sight through the turbulent flow, and is generally referenced as T-ODT. An extension of the model to capture streamwise fluxes of spatially evolving flows (e.g., boundary-layer-type flows) has been presented in [11, 16] and is denoted by S-ODT. More importantly, [16] also present a variable-density formulation for low Mach number flows. In both variable-density T-ODT and S-ODT, a second kernel function $J(y) = |K(y)|$ is introduced in order to facilitate enforcement of physical conservation properties.

For variable-density flow, the various integral expressions above receive the mapped mass density such that $\rho \rightarrow \rho(f(y))$. In variable density T-ODT, the calculation of the available kinetic energy $u_{i,K}$ changes accordingly. The fractions $u_{i,K} / \int_{y_0}^{y_0+l} \rho K^2(y) dy$ and $u_{i,K}^2 / \left(2 \int_{y_0}^{y_0+l} \rho K^2(y) dy \right)$ in

Eqs. (2) and (3), change to $P_i / (2S)$ or $P_i^2 / (4S)$, respectively, where, as in [16],

$$P_i = u_{i,K} - H \int_{y_0}^{y_0+l} [\rho u_i](f(y)) J(y) dy, \quad (6)$$

$$S = \frac{H^2 + 1}{2} \int_{y_0}^{y_0+l} \rho(f(y)) K^2(y) dy - H \int_{y_0}^{y_0+l} \rho(f(y)) J(y) K(y) dy, \quad (7)$$

$$H = \frac{\int_{y_0}^{y_0+l} \rho(f(y)) K(y) dy}{\int_{y_0}^{y_0+l} \rho(f(y)) J(y) dy}. \quad (8)$$

In the S-ODT model, the streamwise change of the scalar profiles in the line-of-sight through turbulence is studied. Two variants arise in this case. One is the conservative boundary-layer formulation [16], and another the non-conservative wall-constrained internal-flow formulation [17]. Essentially, in S-ODT, all integrals in Eqs. (6–8), as well as the integrand of $\int_{y_0}^{y_0+l} \rho K^2(y) dy$ in the prefactor in Eq. (3), receive an additional multiplication by $u(f(y))$, the mapped streamwise advecting velocity (see [16, 17] for details). The time-scale τ changes to a streamwise length-scale ξ , and the temporal sampling Δt_s changes to a streamwise sampling Δx_s [16]. Symbolically, the S-ODT equivalent of Eq. (5) has a modified left-hand side and reads

$$u \frac{\partial u_i}{\partial x} = M_i + K_i + S_i + \nu \frac{\partial^2 u_i}{\partial y^2}. \quad (9)$$

2.4. Extensions to cylindrical geometry

An additional model extension, or a generalization of the T-ODT and S-ODT formulations for both Cartesian and cylindrical flows, considering a dynamically adaptive mesh, was presented in [18]. The cylindrical formulation replaces the planar coordinate y for the radial coordinate r , while any line-integral $\int(\cdot) dy$ in all of the equations presented so far, changes to a surface radial integral of the form $\int(\cdot) r dr$. Eqs. (1) and (9) also consider a change in the form of the gradient flux. The generalized scalar conservation equation, Eq. (1), becomes

$$\frac{\partial \psi}{\partial t} = M(C, Z, r, f(r)) - \frac{1}{r} \frac{\partial (rF(\psi))}{\partial r}, \quad (10)$$

where $F(\psi) = -\sigma(\partial \psi / \partial r)$ for the model resolved radial molecular diffusive flux. The specific form of the viscous flux for every velocity component in the cylindrical coordinate system is given in [17].

Note that [17] also introduces a variable-density formulation in which the density is treated as an active scalar, coupled with the evolution of the temperature. The temperature and density states are coupled by the ideal gas law and the divergence condition during the deterministic evolution between subsequent eddy events. This procedure is the equivalent of the

enforcement of mass and energy conservation.

2.5. Incorporation of EHD effects

Incorporation of EHD effects is done by the implementation of the Coulomb force and the associated electrostatic potential energy in the ODT eddy sampling. The Coulomb force density is given by $\rho_f E_i$, which is a body force to be incorporated in the ODT equations, e.g., Eq. (9) (in such case, per unit fluid density). Here, $\rho_f = e(n_+ c_+ - n_- c_-)$, is the continuum density of free charges due to positive (+) and negative (-) charged species with concentration c_{\pm} and valence n_{\pm} for the unit charge e on an electron. c_{\pm} follow individual scalar conservation equations similar to Eq. (1). E_i denotes the Cartesian components of the electric field vector. By Faraday's law for non-magnetic media, i.e., $E_i = -\partial\Phi/\partial x_i$, where Φ is the total electrostatic potential and $(x_i) = (x, y, z)^T$ the Cartesian coordinates. Coulomb forces in wall-normal direction $i = 2$ do not directly accelerate the flow altogether but influence turbulence properties [19, 4, 8].

The transfer of electrostatic potential energy to kinetic energy, or vice versa, is the mechanism for implementation of the effects of the work performed by the flow against Coulomb forces by a notional eddy turnover that is represented as instantaneous application of the triplet map $f(y)$. This observes a 1-D reduction on the 3-D electric field that aims to capture leading order effects while keeping the flow model self-contained. Hence, only E_2 is resolved that acts along the ODT line in wall-normal (y) direction, which is the direction with the largest property gradients. In that sense, there is no contribution to the kinetic energy by $\rho_f E_i$ by direct Coulomb acceleration. The effect on the mean kinetic energy manifests itself by EHD-enhanced losses due to a modification of the turbulent drag for a fixed mean streamwise pressure gradient force that drives the flow. As detailed before, fluctuating pressure transport is modeled in ODT by the kinetic energy redistribution, i.e., a modification in the Reynolds stress tensor components, which is conceptually comparable to the discussion in [19].

The form of the change in electrostatic potential energy, ΔE_{pot} , results from the work performed on the fluid due to the energy release from the pre-mapped to the post-mapped state analogous to buoyancy [11, 20]. ΔE_{pot} has to be added within the square bracket of Eq. (3) for EHD-enhanced sampling. Likewise, it requires a multiplication by $4S$ under the square root of Eq. (2) for potential energy redistribution due to the ODT kernel. Specializing to Cartesian coordinates, we have

$$\Delta E_{\text{pot}} = - \int_{y_0}^{y_0+l} \left[\rho_f(f(y)) \Phi(\rho_f(f(y))) - \rho_f(y) \Phi(\rho_f(y)) \right] dy. \quad (11)$$

In addition to this and the solution of Eq. (5), the

1-D conservation equation for ρ_f , and the Nernst–Planck equation, are solved together with the 1-D representation of Gauss' law for the electric potential, $\partial(\epsilon E_i)/\partial x_i = \rho_f$, as well as Faraday's law, $E_i = -\partial\Phi/\partial x_i$, for the resolved component $i = 2$ and a known electric permittivity ϵ .

Note that we distinguish two different types of EHD coupling. In the one-way coupling case, the Nernst–Planck equation reduces to a zero-divergence condition for the electric current density [21]. This results then in a uniform electric current density along the ODT line (planar Cartesian case). Electroquasistatic fields are calculated before hand and remain fixed during the simulation. In the case of two-way coupling, the Nernst–Planck equations are similar to Eq. (1). An explicit numerical solver is used in which the model resolved instantaneous profile of $\Phi(y)$ is obtained by numerical solution of a 1-D Poisson equation by application of the Thomas algorithm whenever $\rho_f(y)$ has changed.

3. RESULTS

Turbulent electroconvection exhibits different flow regimes that may be categorized by the relative strengths of the Coulomb, viscous, and inertial forces. In addition, the relaxation processes of free electric charges and their coupling to electric fields within the working fluid need to be taken into account. Typical applications are heat transfer enhancement (e.g. [3]) due to weak coupling and flow control (e.g. [4]) due to strong coupling. Below, we begin with the strongly coupled regime for plane Couette flow of a dilute electrolyte. After that, we turn to the weakly coupled regime for vertical pipe flow with an inner concentric electrode.

3.1. Drag enhancement in turbulent EHD Couette flow

In this section we consider a simple model for strongly coupled wall-bounded EHD turbulence in a Couette-type flow of a dilute electrolyte. The flow configuration is sketched in Figure 1 and corresponds with that in [4]. The top wall is moving and held at a different voltage relative to the bottom one. No-slip isopotential zero-flux wall-boundary conditions are prescribed. The T-ODT model set-up uses $C = 10$, $Z = 600$, $\alpha = 2/3$ as in [22]. The electrolytes considered have neutral bulk charge and consist of two identical ionic scalar species $\psi = c_{\pm}$ with the same valence and mobility but opposite charge. The model-resolved deterministic ion fluxes in accordance with Eq. (1) thus have diffusive and drift contributions so that

$$F_{\pm}(c_{\pm}) = -D \frac{\partial c_{\pm}}{\partial y} \mp \frac{D c_{\pm}}{V_T} \frac{\partial \Phi}{\partial y}. \quad (12)$$

Five dimensionless control parameters define the flow state: the bulk Reynolds number, $\text{Re} = Uh/\nu$, the ionic Schmidt number, $\text{Sc} = \nu/D$, the dimensionless voltage, $\hat{V} = 2V/V_T$, which is varied across the range 1–40, the fixed coupling constant, $\beta =$

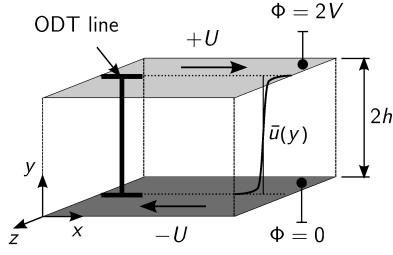


Figure 1. Sketch of the temporally developing EHD Couette flow. The ODT line is fixed in space.

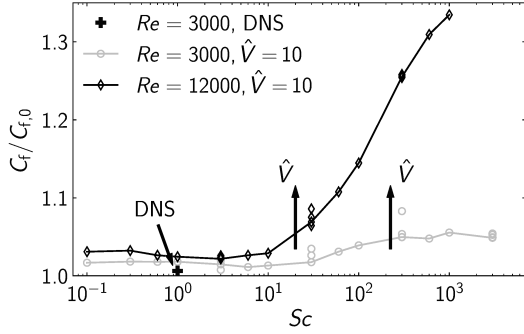


Figure 2. ODT prediction of the turbulent drag enhancement as function of Sc for various Re and voltages. DNS is from [4].

$\epsilon V_T^2 / (\rho \nu D) = 0.5$, and the fixed normalized Debye layer thickness, $\lambda_D / h = \sqrt{\epsilon V_T / (2 \rho c_0 e h^2)} = 0.01$. In these expressions, U denotes the prescribed wall velocity magnitude, h the channel half-height, $V_T = k_B T / e$ the thermal voltage, D the kinematic diffusivity of the ions in the electrolyte, and c_0 the uniform initial concentration of the univalent ion species, respectively, in addition to the other physical parameters introduced above.

Figure 2 shows the skin friction drag coefficient C_f , which is, for Couette flow, evaluated based on the Reynolds-averaged streamwise velocity profile, $\bar{u}(y) = u(y, t)$, as

$$C_f = 2 \frac{u_\tau^2}{U^2} \quad \text{with} \quad u_\tau = \sqrt{\nu \left| \frac{d\bar{u}}{dy} \right|_{\text{wall}}}. \quad (13)$$

ODT pre-simulations conducted for $\hat{V} = 0$ (absence of EHD effects; not shown here) agree with corresponding purely hydrodynamic reference experiments [23] within 2–5% yielding $C_{f,0} \approx 5.9 \times 10^{-3}$ for $Re = 3000$ and $C_{f,0} \approx 4.7 \times 10^{-3}$ for $Re = 12,000$, respectively. This level of agreement is also exhibited by the EHD-enhanced cases at $Sc \approx 1$ that only mildly overestimate available reference DNS as shown in Fig. 2. In fact, present ODT results suggest that the turbulent drag is largely insensitive to EHD effects for $Sc \lesssim 10$.

A significant increase of the turbulent drag can be seen in Fig. 2 for $Sc \gtrsim 30$ up to $\approx 30\%$ for $Sc \geq 300$ at $Re = 12,000$ investigated. The mag-

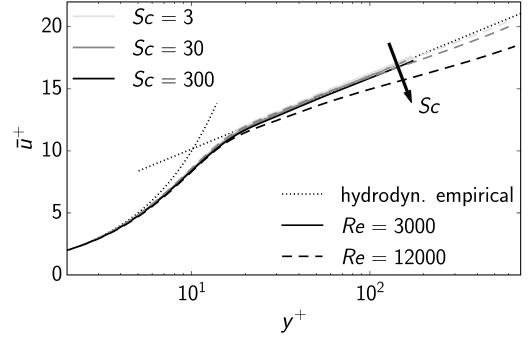


Figure 3. ODT resolved mean velocity in the boundary layer for various Re and Sc but fixed voltage. The empirical law of the wall (e.g. [25]) for hydrodynamic flow without EHD effects is given for orientation.

nitude of the effect increases with Sc , Re , and \hat{V} . Interestingly, ODT predicts a regime change for the critical Schmidt number $Sc_{\text{crit}} \approx 30$, which agrees with an inferred value of $Sc_{\text{crit}} \sim O(10)$ suggested by [4] based on DNS, albeit it remained elusive if drag increases or decreases due to enhanced coupling. In any case, the ODT prediction suggests that Re must be large enough so that the turbulent scaling cascade is broad enough to be sensibly influenced by EHD effects [24].

Figure 3 shows wall-normal profiles of the dimensionless mean velocity deficit \bar{u}^+ over the dimensionless boundary layer coordinate y^+ given by

$$\bar{u}^+ = \frac{|\bar{u} - u_{\text{wall}}|}{u_\tau}, \quad y^+ = \frac{y u_\tau}{\nu}. \quad (14)$$

ODT simulation results are shown for various Re and Sc but fixed $\hat{V} = 4$ in order to assess which region is influenced by EHD effects. The hydrodynamic law of the wall (e.g. [25]) is given here by the viscous sub and log layers, $\bar{u}^+(y^+) = y^+$ for $y^+ < 5$ and $\bar{u}^+(y^+) = \kappa^{-1} \ln y^+ + B$ with $\kappa = 0.39$ and $B = 4.2$ for $y^+ > 30$, respectively. Boundary layer similarity is broken first in the bulk and outer layer for the ODT simulations with $Re = 12,000$ and $Sc = 30$ shown. For further increasing Sc , the entire log region is affected. Decreasing \bar{u}^+ for increasing Sc reflects the increase in u_τ due to which C_f increases so that the trend in Fig. 3 is consistent with that in Fig. 2.

ODT is a high-fidelity flow model that predicts sensible mean effects in two-way coupled EHD turbulence for at least moderately high Re and Sc . This regime is presently inaccessible to DNS and not faithfully treatable with LES or RANS due to the modeling involved. A 3-D extension of the stochastic model (e.g., based on [26]) and dedicated reference experiments are needed in order to assess the 1-D model prediction in order to clarify its applicability to EHD turbulence.

3.2. Drag enhancement in turbulent EHD vertical pipe flow

In this section we present the results for a one-way coupled EHD pipe flow simulation with an inner concentric electrode, which resembles the experimental electrostatic precipitator (ESP) device of [27]. The flow configuration sketch is shown in Figure 4. In the ODT simulations, the radially oriented S-ODT line is advected upwards with the flow through the ESP. The cylindrical pipe flow is subject to an electric field induced by a (positive) corona discharge originated at the electrode. We only consider one-way coupled electric fields which are not modified by fluctuations in ρ_f , yet equally affect the stochastic random sampling as described in Sec. 2.5. Electric charges (positive ions in air) are assumed as a continuum phase. For details on the generation of the electroquasistatic (EQS) fields and on the general implementation, please refer to [28]. In addition to the electrostatic potential energy formulation used during eddy events, we also incorporate the Joule heating as a source term to resolve during the deterministic advancement of the temperature equation, see [28].

The objective of the simulations is the evaluation of the friction drag, which is represented in [27] by the Darcy friction factor f_D ,

$$f_D = -\frac{4R}{\rho_b U_b^2} \frac{d\bar{p}}{dz}. \quad (15)$$

For the axially symmetric mean flow, $d\bar{p}/dz$ can be obtained from the Reynolds-averaged momentum equations, neglecting turbulent correlations of the molecular dynamic viscosity. Indeed, the wall pressure difference, between the outlet and the inlet of the pipe section, can be calculated as

$$\begin{aligned} \Delta p_w = & -\frac{2}{R^2} \Delta \left[\int_0^R \langle \rho u_1 u_1 \rangle r dr - R^2 \left(\langle \mu \rangle \frac{\partial \langle u_2 \rangle}{\partial r} \right) \Big|_R \right] \\ & -\frac{2}{R^2} \Delta \left[\int_0^R \langle \mu \rangle \frac{\partial \langle u_2 \rangle}{\partial r} r dr \right] - \frac{2}{R} \int_0^{B_{TS}} \tau_w dz \\ & - \frac{J_R}{\beta_f}. \end{aligned} \quad (16)$$

Here, Δ refers to a difference between the outlet ($z = B_{TS}$) and the inlet ($z = 0$) of the simulated device. J_R is the uniform radially weighted electric current density, which is obtained from the voltage-current values given as an input to the simulation, and β_f is the mobility of the free ionic charges. Eq. (16) allows an approximation of the average pressure gradient required for Eq. (15) as $d\bar{p}/dz \approx \Delta p_w / B_{TS}$.

Figure 5 shows the ensemble average of the inlet profiles used in the S-ODT simulations. Two different types of profiles are used based on the geometry of the experimental device. Unlike a traditional pipe flow, the configuration in Fig. 4 includes an internal electrode boundary, which imposes a no-

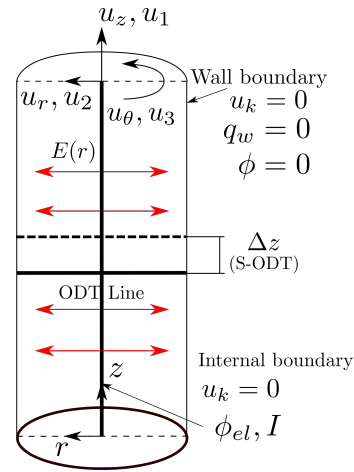


Figure 4. Sketch of the spatially developing EHD vertical pipe flow. The ODT line is advected upwards with the flow.

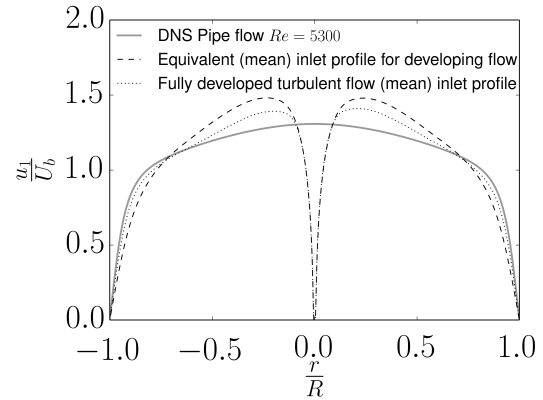


Figure 5. Ensemble average of initial (inlet) conditions for the evaluated $Re = 4000$ pipe flow (see description in text). Reference DNS data by [29] is shown for comparison.

slip condition at the electrode. Note that the sketch provided in Fig. 4 corresponds to the test section of the experimental device, see [27]. The device possesses an entry section, which is supposed to provide a fully developing flow at the inlet of the test section. However, a verification of the hydrodynamic entry length L_H (see [30]) performed for one of the Reynolds number cases in [27], $Re_b = 4000$, shows that L_H is larger than the sum of both device entry and test section lengths. Therefore, we evaluate both fully developed turbulent inlet profiles (generated with a cylindrical T-ODT formulation), as well as equivalent turbulent flow profiles achieving a target developing f_D value. The latter is calculated according to the actual entry and test section lengths, and the formula provided in [30].

Figure 6 shows the results for the evaluation of f_D . The experimental device has radius $R = 1.6 \times 10^{-2}$ m, test section length $B_{TS} = 1.02$ m, and entry section length $B_{entry} = 1.59$ m. The in-

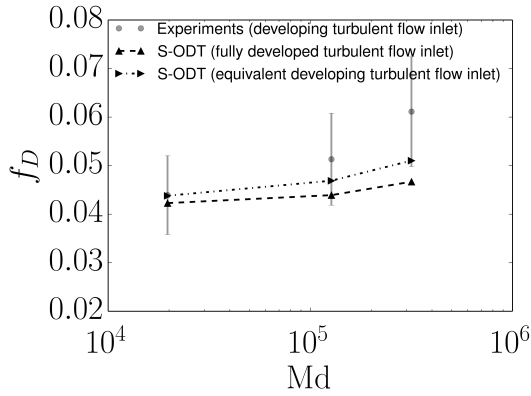


Figure 6. ODT prediction of Darcy friction factor enhancement with dimensionless EHD body force (Md). Reference experiments are from [27].

ner concentric electrode of the device has radius $R_{elec} = 1.25 \times 10^{-4}$ m, and length $B_{elec} = 2.05$ m. The inlet gas flow is assumed at atmospheric pressure with uniform fluid properties (Prandtl number $Pr_{air} \approx 0.71$) at a temperature $T_0 = 300.15$ K. The inlet flow has a bulk velocity $U_b = 2$ m/s, and associated $Re_b = 4000$. We evaluate three different Masuda numbers, $Md \approx 1.97 \times 10^4$, 1.27×10^5 , and 3.17×10^5 , on top of the neutral (no EHD) pipe flow condition. Note that $Md = \epsilon_0 \Phi_{el} (\Phi_{el} - \Phi_{on}) / (\rho_0 \nu_0^2)$, where ϵ_0 is the vacuum electrical permittivity, Φ_{el} the electrode operating voltage, and Φ_{on} the corona-discharge onset voltage (both voltages are measured in the experiments).

Despite the friction factor evaluation being simply an integral quantity of the flow, the results obtained by the ODT simulations (see Fig. 6) are worth commenting due to the multiphysical nature of the application. This is neither an application that can be easily evaluated by DNS nor treated faithfully with LES or RANS. ODT provides small-scale resolution and dynamical complexity by capturing relevant physical processes at feasible cost. The relative contributions to the pressure gradient according to Eq. (16) are thus model predictions. It has been verified that the largest contribution to $d\bar{p}/dz$ is due to the wall shear stress τ_w , and in second place, by the average kinetic energy gradient. The latter is the reason why the utilization of developing flow inlet conditions are necessary to obtain a model prediction that reasonably captures the reference experiments.

4. SUMMARY

EHD turbulence denotes a chaotic flow that is influenced by inertial, viscous, and Coulomb forces across a range of scales. Dynamical processes are nonuniversal and reach down to the Kolmogorov scale [7], η_K , and Batchelor scales [31], $Sc^{-1/2}\eta_K$, placing a strong burden on numerical simulation and modeling. Small-scale resolution is addressed by utilizing the stochastic One-Dimensional Turbulence

(ODT) model for regime-overreaching numerical investigation of wall-bounded EHD-enhanced flows.

For two-way coupled EHD Couette flow, ODT predicts EHD-enhanced outer layer turbulence that nonlocally affects the entire turbulent boundary layer. Turbulent drag increases for $Re \gtrsim 10^4$ and $Sc \gtrsim 30$ suggesting that charge carriers need to sample the turbulent microstructure exhibiting $\sqrt{Sc} \gtrsim 5$ times smaller length scales than the velocity field.

In one-way coupled vertical EHD pipe flow with a coaxial central electrode, ODT hints at transient effects in a developing turbulent flow. Turbulent drag is enhanced by an EHD-based amplification of the rate of change of the turbulent kinetic energy as revealed by an analysis of the contributions to the pressure drop per unit pipe length.

Altogether, ODT is a self-contained, dimensionally reduced flow model that combines fidelity, predictability, and numerical efficiency. We have demonstrated its applicability to EHD-enhanced flows for future application as sub-filter-scale model.

ACKNOWLEDGEMENTS

H.S., J.M., and M.K. acknowledge support by the European Regional Development Fund (EFRE), Grant no. StaF 23035000. Furthermore, M.K. acknowledges support by the BTU Graduate Research School (Conference Travel Grant).

REFERENCES

- [1] Robinson, M., 1968, ‘‘Turbulent Gas Flow and Electrostatic Precipitation’’, *J Air Pollut Control Assoc*, Vol. 18 (4), pp. 235–239.
- [2] Laohalerdecha, S., Naphon, P., and Wongwises, S., 2007, ‘‘A review of electrohydrodynamic enhancement of heat transfer’’, *Renewable Sustainable Energy Rev*, Vol. 11 (5), pp. 858–876.
- [3] Bacher, C., and Riebel, U., 2021, ‘‘Electrohydrodynamically enhanced mass transfer in a wetted-wall column’’, *Chem Eng Res Des*, Vol. 167, pp. 183–197.
- [4] Ostilla-Mónico, R., and Lee, A. A., 2017, ‘‘Controlling turbulent drag across electrolytes using electric fields’’, *Faraday Discuss*, Vol. 199, pp. 159–173.
- [5] Shiva Kumar, S., and Himabindu, V., 2019, ‘‘Hydrogen production by PEM water electrolysis – A review’’, *Mater Sci Energy Technol*, Vol. 2 (3), pp. 442–454.
- [6] Ju, Y., and Sun, W., 2015, ‘‘Plasma assisted combustion: Dynamics and chemistry’’, *Prog Energy Combust Sci*, Vol. 48, pp. 21–83.
- [7] Kolmogorov, A. N., 1941, ‘‘The local structure of turbulence in incompressible viscous fluid for very large Reynolds numbers’’, *Dok Akademi Nauk SSSR*, Vol. 30, pp. 299–303.

- [8] Zhao, W., and Wang, G., 2017, “Scaling of velocity and scalar structure functions in AC electrokinetic turbulence”, *Phys Rev E*, Vol. 95 (2), 023111.
- [9] Storey, B. D., 2005, “Direct numerical simulation of electrohydrodynamic flow instabilities in microchannels”, *Phys D: Nonlin Phen*, Vol. 211 (1), pp. 151–167.
- [10] Duraisamy, K., Iaccarino, G., and Xiao, H., 2019, “Turbulence Modeling in the Age of Data”, *Annu Rev Fluid Mech*, Vol. 51 (1), pp. 357–377.
- [11] Kerstein, A. R., 1999, “One-dimensional turbulence: Model formulation and application to homogeneous turbulence, shear flows, and buoyant stratified flows”, *J Fluid Mech*, Vol. 392, pp. 277–334.
- [12] Klein, M., Schmidt, H., and Lignell, D. O., 2022, “Stochastic modeling of surface scalar-flux fluctuations in turbulent channel flow using one-dimensional turbulence”, *Int J Heat Fluid Flow*, Vol. 93, 108889.
- [13] Papoulis, A., and Pillai, S. U., 2002, *Probability, Random Variables, and Stochastic Processes*, McGraw-Hill, New York, 4th edn.
- [14] Kerstein, A. R., Ashurst, W. T., Wunsch, S., and Nilsen, V., 2001, “One-dimensional turbulence: Vector formulation and application to free-shear flows”, *J Fluid Mech*, Vol. 447, pp. 85–109.
- [15] Lee, K., Venugopal, V., and Girimaji, S. S., 2016, “Pressure-strain energy redistribution in compressible turbulence: Return-to-isotropy versus kinetic-potential energy equipartition”, *Phys Scr*, Vol. 91 (8), 084006.
- [16] Ashurst, W. T., and Kerstein, A. R., 2005, “One-dimensional turbulence: Variable-density formulation and application to mixing layers”, *Phys Fluids*, Vol. 17 (2), 025107.
- [17] Medina Méndez, J. A., Klein, M., and Schmidt, H., 2019, “One-Dimensional Turbulence investigation of variable density effects due to heat transfer in a low Mach number internal air flow”, *Int J Heat Fluid Flow*, Vol. 80, 108481.
- [18] Lignell, D., Lansinger, V. B., Medina Méndez, J. A., Klein, M., Kerstein, A. R., Schmidt, H., Fistler, M., and Oevermann, M., 2018, “One-dimensional turbulence modeling for cylindrical and spherical flows: model formulation and application”, *Theor Comput Fluid Dyn*, Vol. 32 (4), pp. 495–520.
- [19] Davidson, J. H., and Shaughnessy, E. J., 1986, “Turbulence generation by electric body forces”, *Exp Fluids*, Vol. 4 (1), pp. 17–26.
- [20] Wunsch, S., and Kerstein, A. R., 2005, “A stochastic model for high-Rayleigh-number convection”, *J Fluid Mech*, Vol. 528, pp. 173–205.
- [21] Melcher, J. R., 1981, *Continuum electromechanics*, Vol. 2, MIT press Cambridge.
- [22] Klein, M., and Schmidt, H., 2020, “Towards a stochastic model for electrohydrodynamic turbulence with application to electrolytes”, *Proc Appl Math Mech*, Vol. 20, e202000128.
- [23] Robertson, J. M., 1959, “On turbulent plane Couette flow”, *Sixth Midwestern Conference on Fluid Mechanics*, University of Texas, Austin, pp. 169–182.
- [24] Klein, M., and Schmidt, H., 2021, “Investigating Schmidt number effects in turbulent electroconvection using one-dimensional turbulence”, *Proc Appl Math Mech*, Vol. 21, e202100147.
- [25] Pope, S. B., 2000, *Turbulent Flows*, Cambridge University Press, ISBN 978-0521598866.
- [26] Glawe, C., Medina M., J. A., and Schmidt, H., 2018, “IMEX based multi-scale time advancement in ODTLES”, *Z Angew Math Mech*, Vol. 98, pp. 1907–1923.
- [27] Nelson, D. A., Ohadi, M. M., Zia, S., and Whipple, R. L., 1990, “Electrostatic effects on pressure drop in tube flows”, *Int J Heat Fluid Flow*, Vol. 11 (4), pp. 298–302.
- [28] Medina Méndez, J. A., 2020, “Application of the One-Dimensional Turbulence model to electrohydrodynamically enhanced internally forced convective flows”, Ph.D. thesis, Brandenburgische Technische Universität Cottbus-Senftenberg, Cottbus, Germany.
- [29] Khoury, G. K. E., Schlatter, P., Noorani, A., Fischer, P. F., Brethouwer, G., and Johansson, A. V., 2013, “Direct Numerical Simulation of Turbulent Pipe Flow at Moderately High Reynolds Numbers”, *Flow, Turbul Comb*, Vol. 91 (3), pp. 475–495.
- [30] Abraham, J. P., Sparrow, E. M., and Tong, J. C. K., 2008, “Breakdown of Laminar Pipe Flow into Transitional Intermittency and Subsequent Attainment of Fully Developed Intermittent or Turbulent Flow”, *Numer Heat Transfer, Part B*, Vol. 54 (2), pp. 103–115.
- [31] Batchelor, G. K., 1959, “Small-scale variation of convected quantities like temperature in turbulent fluid. Part 1. General discussion and the case of small conductivity”, *J Fluid Mech*, Vol. 5, pp. 113–133.